Recombination activity of light-activated copper defects in *p*-type silicon studied by injection- and temperature-dependent lifetime spectroscopy

Alessandro Inglese,[1,a)] Jeanette Lindroos,[2] Henri Vahlman,[1] and Hele Savin[1]
[1]*Department of Micro- and Nanosciences, Aalto University, Tietotie 3, 02150 Espoo, Finland*
[2]*Department of Engineering and Physics, Karlstad University, Universitetsg. 2, 65188 Karlstad, Sweden*

(Received 1 July 2016; accepted 7 September 2016; published online 26 September 2016)

The presence of copper contamination is known to cause strong light-induced degradation (Cu-LID) in silicon. In this paper, we parametrize the recombination activity of light-activated copper defects in terms of Shockley—Read—Hall recombination statistics through injection- and temperature dependent lifetime spectroscopy (TDLS) performed on deliberately contaminated float zone silicon wafers. We obtain an accurate fit of the experimental data via two non-interacting energy levels, i.e., a deep recombination center featuring an energy level at $E_c - E_t = 0.48 - 0.62\,\text{eV}$ with a moderate donor-like capture asymmetry ($k = 1.7 - 2.6$) and an additional shallow energy state located at $E_c - E_t = 0.1 - 0.2\,\text{eV}$, which mostly affects the carrier lifetime only at high-injection conditions. Besides confirming these defect parameters, TDLS measurements also indicate a power-law temperature dependence of the capture cross sections associated with the deep energy state. Eventually, we compare these results with the available literature data, and we find that the formation of copper precipitates is the probable root cause behind Cu-LID. *Published by AIP Publishing.*
[http://dx.doi.org/10.1063/1.4963121]

I. INTRODUCTION

Light-induced degradation (LID) is a current topic in silicon photovoltaics research due to its deleterious impact on solar cell efficiency upon exposure to illumination. This phenomenon has been traditionally ascribed to the formation of metastable boron-oxygen (B-O) complexes, whose composition has been intensively debated in the literature.[1,2] However, recent results that showed severe LID in solar cells fabricated from multicrystalline silicon substrates[3,4] with low bulk oxygen content have raised numerous discussions on alternative defect reactions, which might explain the observed degradation process. Low levels of copper contamination have been recently shown to cause a similar LID effect in both mono-[5] and multi crystalline silicon.[6,7] This phenomenon is referred to as copper-related light-induced degradation (Cu-LID), and it has been suggested to arise from increased bulk recombination[8–10] caused by copper precipitation[11,12] or substitutional copper complexes.[13–15] Nevertheless, the recombination mechanisms at Cu-LID defects still remain unclear, and the current literature information is lacking in an accurate parametrization of the recombination activity of such defects. Therefore, it is important to determine the recombination parameters of Cu-LID defects in order to quantify their effect on minority carrier lifetime and predict their impact on the overall solar-cell performance.

Lifetime spectroscopy (LS) has been proposed in the literature as an effective approach to characterize electrically active defects through standard minority carrier lifetime measurements.[16,17] LS techniques are based on the analysis of the injection- and temperature dependence of the minority carrier lifetime in terms of Shockley—Read—Hall (SRH) recombination statistics,[18,19] such that the recombination parameters of the lifetime-limiting defect can be directly determined from least-squares fits to the experimental data. Since carrier lifetime is one of the most sensitive parameters to the presence of electrically active defects, LS methods enable the characterization of recombination active defects with concentrations well below the detection limit of other well-established characterization techniques, e.g., deep level transient spectroscopy (DLTS).

This paper aims at gaining a deeper insight into the recombination activity of the defect behind Cu-LID and the associated recombination phenomena. In this contribution, we apply LS methods to determine the SRH recombination parameters of light-activated Cu defects in deliberately contaminated float zone silicon (FZ-Si) wafers, which are free of B-O recombination due to the low bulk oxygen concentration. Since SRH parameters represent a typical fingerprint of the underlying recombination active defect, the extracted defect parameters have been compared with literature data, in order to correlate the LS results with the existing information on electrically active copper complexes.

II. EXPERIMENTAL

A. Sample preparation

The experiments were conducted on B-doped, 4-in., [100]-oriented FZ-Si wafers with the thickness of 280 μm and resistivity of 0.9, 3.4, and 18.4 $\Omega\cdot$cm. After standard RCA-1 and RCA-2 cleanings, the wafer surfaces were passivated by growing a 15 nm thick thermal oxide layer, which was formed during 40 min of dry oxidation at 900 °C followed by annealing in nitrogen ambient at the same temperature for 20 min. Some wafers were then kept as reference samples, while the rest of the batch was subjected to intentional copper

a)E-mail: alessandro.inglese@aalto.fi

RIGHTSLINK

contamination, performed by spinning a 1 ppm copper sulfate solution and subsequently annealing the samples in a nitrogen atmosphere at 800 °C for 20 min. This procedure resulted in bulk interstitial copper contamination, whose concentration is estimated to be in the range of 10^{14} cm^{-3}. Next, an external corona charge was deposited on both wafer sides (+0.3 μC/cm^2) to prevent Cu out-diffusion and decrease the surface minority carrier recombination through the formation of an inversion layer near the surface. The samples were then exposed to room temperature illumination under a 0.5 Sun LED lamp for up to 130 h in order to induce LID until the achievement of complete lifetime saturation. During light soaking, the lifetime decay caused by Cu-LID was constantly recorded as a function of illumination time through automated quasi-steady state photoconductance decay (QSSPC) measurements.

B. Injection and temperature-dependent lifetime measurements

Minority carrier lifetime measurements were performed by means of a Sinton WCT 120-TS tester, which allows injection-dependent QSSPC lifetime measurements at temperatures between 20 °C and 200 °C. The measurement setup consists of an inductive RF coil incorporated within a thermocouple-controlled measurement stage. Temperature-dependent measurements were performed by initially heating the measurement stage up to the maximum temperature and subsequently measuring the lifetime after predefined temperature steps of the cooling transient. Since carrier mobility strongly depends on the temperature, a correction based on Dorkel–Leturcq's mobility model[20] was applied to ensure the optimal calibration of the instrument over the whole temperature range. Furthermore, as the QSSPC technique is prone to trapping artifacts at low injection conditions,[22] measurement points featuring abnormal lifetime increase at excess carrier concentrations below 10^{14} cm^{-3} were excluded from the analysis of the experimental data.

III. MODELING OF THE EXPERIMENTAL DATA

The SRH theory provides a well-established statistical model for describing charge carrier recombination at single energy levels within the bandgap, and it constitutes the conceptual framework behind lifetime spectroscopy methods. The determination of defect parameters through lifetime spectroscopy is thus performed under the assumption that the unknown recombination active defect introduces discrete energy levels. Supposing negligible trapping and, hence, equal excess electron and hole concentration ($\Delta n = \Delta p$), the SRH lifetime τ_{SRH} associated with a single-level defect is given by the following well-known equation:[21]

$$\tau_{SRH}(\Delta n, T) = \frac{\tau_{n0}(p_0 + p_1 + \Delta n) + \tau_{p0}(n_0 + n_1 + \Delta n)}{p_0 + n_0 + \Delta n}, \tag{1}$$

where n_0 and p_0, respectively, represent the equilibrium electron and hole concentrations and the capture time constants τ_{n0} and τ_{p0} are related to the defect density N_t, the thermal velocity v_{th}, and the electron and hole capture cross sections σ_n and σ_p via $\tau_{n0} = (N_t v_{th} \sigma_n)^{-1}$ and $\tau_{p0} = (N_t v_{th} \sigma_p)^{-1}$. The quantities n_1 and p_1 are often referred to as SRH densities and represent the electron and hole concentrations when the defect energy level E_t coincides with the Fermi level, i.e.,

$$n_1(E_t, T) = N_c \exp\left(-\frac{E_c - E_t}{kT}\right) \quad \text{and}$$
$$p_1(E_t, T) = N_v \exp\left(-\frac{E_t - E_v}{kT}\right), \tag{2}$$

where E_c and E_v are the energetic positions of the conduction and valence bands and N_c and N_v are the effective densities of states in the conduction and valence bands, respectively. The recombination center is, thus, defined via three fundamental parameters, i.e., τ_{n0}, τ_{p0}, and E_t, which must be simultaneously fitted from the injection and temperature-dependent experimental data. When the effect of two or more energy levels is taken into account, the total SRH lifetime is calculated as a reciprocal sum of the inverse lifetimes given by each recombination center.

The injection-dependent lifetime spectroscopy (IDLS) consists of the determination of the defect parameters by fitting Eq. (1) to the injection-dependent lifetime curves. Since the IDLS alone often yields ambiguous results, the analysis must be complemented with the temperature-dependent lifetime spectroscopy (TDLS). In this case, Eq. (1) is fitted to the temperature-dependent lifetime data measured at fixed injection level. The major contribution to the overall temperature dependence arises from the exponential dependence of n_1 and p_1. However, since Eq. (2) includes the state density N_c and N_v, the variation of these two parameters as a function of temperature must also be taken into account, i.e.,

$$N_C(T) = N_C^{300\,K}\left(\frac{T}{300\,K}\right)^{1.5} \quad \text{and}$$
$$N_V(T) = N_V^{300\,K}\left(\frac{T}{300\,K}\right)^{1.5}, \tag{3}$$

where the effective densities of states are taken as $N_c^{300K} = 2.86 \times 10^{19}$ cm^{-3} and $N_v^{300K} = 3.1 \times 10^{19}$ cm^{-3}.[23] Additional temperature-dependence is imposed by the capture time constants τ_{n0} and τ_{p0} via the capture cross sections σ_n and σ_p, whose variation mainly depends on the recombination mechanisms at the defect, and the carrier thermal velocity v_{th}, which has been parametrized as follows:

$$v_{th}(T) = v_{th}^{300\,K}\left(\frac{T}{300\,K}\right)^{0.5} \tag{4}$$

with $v_{th}^{300K} = 1.1 \times 10^7$ cm/s being the thermal velocity of carriers at 300 K. As a first approximation, σ_n and σ_p are assumed to be temperature independent. Since a single set of defect parameters must provide an optimum fit to all the temperature- and injection-dependent lifetime curves, the temperature-dependence of σ_n and σ_p has been subsequently introduced in order to resolve possible inconsistencies between the fit results obtained from IDLS and TDLS analyses.

RIGHTSLINK

IV. RESULTS

A. Degradation process and determination of Cu-related lifetime

Figure 1 presents the effective lifetime measured during room-temperature illumination in an intentionally Cu-contaminated 3.4 Ω·cm FZ sample. The absence of LID in the reference sample indicates that the lifetime decay observed with intentionally contaminated specimens is solely caused by copper impurities. The Cu-related degradation process in FZ-Si occurs via a single asymptotical degradation process, which leads to complete lifetime saturation after at least 50 h of uninterrupted illumination. In this work, defect characterization has been carried out after complete lifetime saturation, such that the characterization of the defect is performed during its most harmful and recombination active state.

In order to obtain reliable spectroscopic results, the bulk lifetime limited by recombination at copper defects must always be separated from the effect of other recombination mechanisms, e.g., Auger, radiative, and surface recombination. Since no LID is observed in the reference sample, it can be reasonably assumed that light soaking solely activates Cu-LID defects while leaving the other recombination mechanisms unchanged. Therefore, the effective Cu-related lifetime (τ_{Cu-eff}) can be calculated as follows:

$$\tau_{Cu-eff} = \left(\frac{1}{\tau_{Cu-deg}} - \frac{1}{\tau_{ref}}\right)^{-1}, \quad (5)$$

where τ_{Cu-deg} and τ_{ref} are the minority carrier lifetimes measured after light soaking in the intentionally Cu-contaminated and the clean reference sample, respectively.

Figure 2 shows the lifetime values of τ_{Cu-deg}, τ_{ref}, and τ_{Cu-eff} plotted against the excess carrier densities. The superposition of the curves representing τ_{Cu-deg} and τ_{Cu-eff} over a broad injection range proves that the measured lifetime is largely dominated by carrier recombination through light-activated copper defects. Note that, in Eq. (5), the lifetime measured before illumination τ_{init} can, in principle, be used in lieu of τ_{ref} for the determination of the effective Cu-related lifetime. The figure also displays the Cu-related lifetime calculated by means of τ_{init} and τ_{ref}. Despite the slight shift between τ_{init} and τ_{ref}, which is probably caused by the effect of the contamination procedure on surface and Auger recombination, the superposition of the lifetime curves obtained from these two methods indicates that both of them can be used to determine the actual Cu-related lifetime. Since the latter approach would require the accurate measurement of τ_{init} at varying temperatures, which may turn interstitial copper into a recombination active state before light soaking,[9,13,24] in this work, τ_{Cu} has been calculated by compensating the lifetime measured after degradation with temperature-dependent lifetime data obtained from a separate non-contaminated reference specimen.

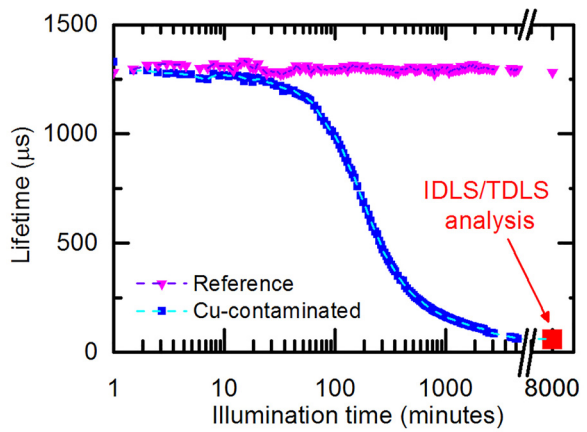

FIG. 1. Minority carrier lifetime measured at a fixed injection level ($\Delta n = 1 \times 10^{14}$ cm^{-3}) as a function of the illumination time measured in a clean reference (magenta) and 1 ppm Cu-contaminated (blue) FZ-Si sample with the resistivity of 3.4 Ω·cm.

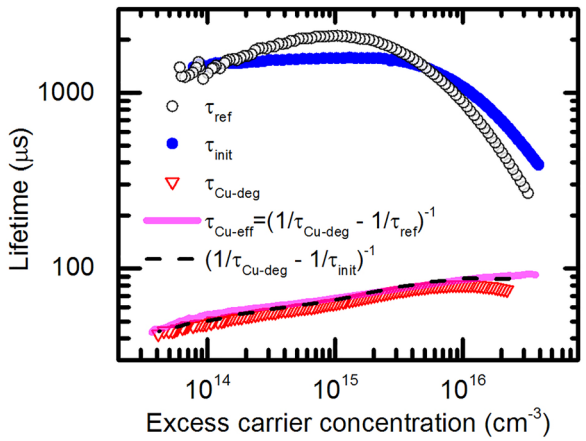

FIG. 2. Minority carrier lifetime measured after degradation (τ_{Cu-deg}—open red triangles) with an intentionally Cu-contaminated 3.4 Ω·cm FZ wafer and in an analogous clean reference specimen (τ_{ref}—open white circles). The image also reports the lifetime curve measured in the contaminated specimen before light soaking (τ_{init}—filled blue circles) and the effective copper-related SRH lifetime calculated by compensating τ_{Cu-deg} with τ_{ref} (solid pink line) and τ_{init} (dashed black line). The slight shift between τ_{init} and τ_{ref} does not significantly affect the calculation of the effective Cu-related lifetime, as indicated by the superposition of the dashed black curve with the effective lifetime values calculated with (5).

B. Parametrization of the Cu-related lifetime in terms of SRH statistics

Figure 3 shows the injection-dependent lifetime curves in the temperature range from 25 to 195 °C and the corresponding SRH fit to the measured lifetime data. The SRH fit of the entire set of injection- and temperature dependent lifetime curves requires the assumption of two non-interacting energy states, i.e., a deep recombination center, which mostly dominates the lifetime curve at a low injection level, and an additional shallow energy level affecting the carrier lifetime only at high injection conditions.

Since the coexistence of two defect centers unavoidably increases the number of parameters that must be simultaneously determined from each fit, the fit procedure was divided into several steps. As it will be discussed below in Fig. 4, the optimum fit of the low-injection part of each lifetime curve is achieved through a wide range of the defect parameters associated with the deep recombination center. Therefore, in an initial step, the defect parameters of the

RIGHTSLINK

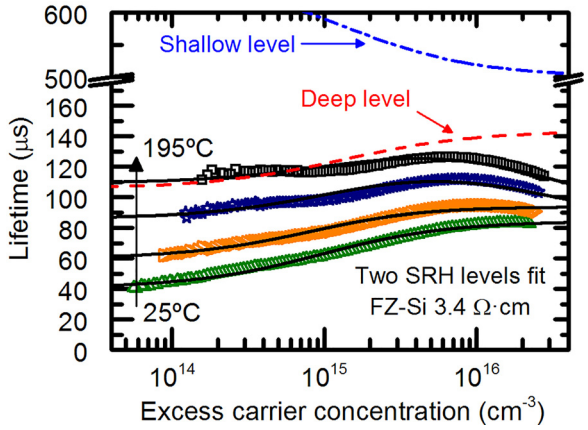

FIG. 3. SRH fit (solid lines) of the injection-dependent lifetime data (symbols) measured at varying temperatures with an intentionally Cu-contaminated p-type FZ-wafer. The lifetime data have been modeled assuming a deep (dashed red line) recombination center with the defect parameters determined in Figure 5 and a shallow (dashed-dotted blue line) recombination center located at $E_c - E_t = 0.15$ eV with k = 0.1.

shallow recombination center were initially optimized to fit the high injection part of the whole set of lifetime curves and the parameters associated with the deep level were arbitrarily chosen from the ranges that guarantee the optimum fit to the experimental data. Subsequently, the parameters of the shallow energy level were kept on fixed values ($E_c - E_t = 0.15$ eV with $k = 0.1$) and the true parameters associated with the deep recombination center were determined through the defect parameter solution surface (DPSS) method proposed by Rein *et al.*[25,26] This approach consists of a fit routine which calculates the optimal fit values of the symmetry factor $k = \frac{\tau_{p0}}{\tau_{n0}} = \frac{\sigma_n}{\sigma_p}$ and τ_{n0} associated with the deep recombination center, while varying the values of the defect energy level E_t across the whole bandgap. Figure 4 shows an example of DPSS analysis applied to a single IDLS curve measured at room temperature, where the fitted *k*-factors are plotted together with the

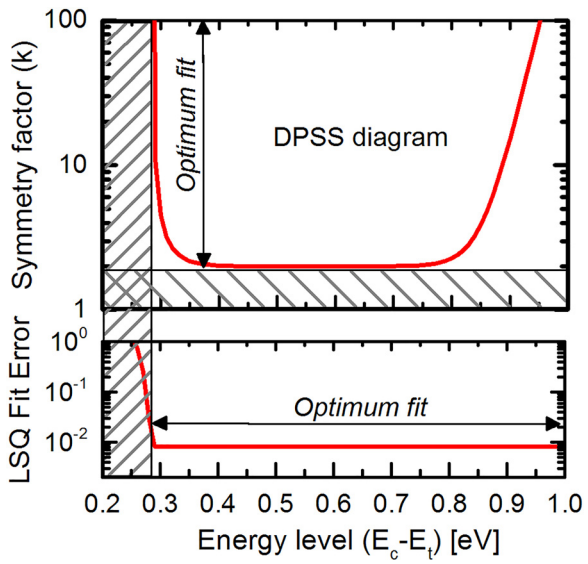

FIG. 4. DPSS diagram of a single IDLS curve measured at room temperature. The fit error is assessed by calculating the optimal fit parameters for each energy level. The fit result shown in the diagram sets a lower bound for the energy level ($E_c - E_t > 0.28$ eV) and the symmetry factor ($k > 2$).

least-squares fit error for each energy level E_t. It results clear that the analysis of a single injection-dependent lifetime curve leads to rather ambiguous fit results, as the least squares fit error is minimized by a broad range of different defect parameters. Such ambiguity can be overcome by extending the DPSS to the whole set of temperature-dependent lifetime curves and superposing the corresponding DPSS curves in the same graph, as shown in Figure 5(a). In this case, the optimal values of the defect parameters are identified by the convergence of all DPSS curves into a common intersection point. The displacement between the DPSS curves has been quantified in terms of relative standard deviation of the DPSS-*k* values at each energy level E_t, which is plotted in Figure 5(b). The relative standard deviation presents two distinct minima located at $E_c - E_t = 0.48 \pm 0.01$ eV and $E_c - E_t = 0.62 \pm 0.02$ eV. Hence, the large ambiguity arising from the SRH fit of a single IDLS curve results to be confined to a relatively narrow energy range located across the mid-bandgap, whose boundaries represent the optimal fit parameters. The minima of the calculated relative standard deviation also allow us to estimate the value of the symmetry factor, which results to be unambiguously determined as $k = 1.7 \pm 0.4$.

As discussed in Ref. 25, the superposition of all the temperature-dependent DPSS curves significantly reduces the ambiguity of the fit result obtained from a single IDLS curve. However, this method does not allow us to determine which of the two intersection points correspond to the exact defect parameters due to the reduced sharpness of the intersection

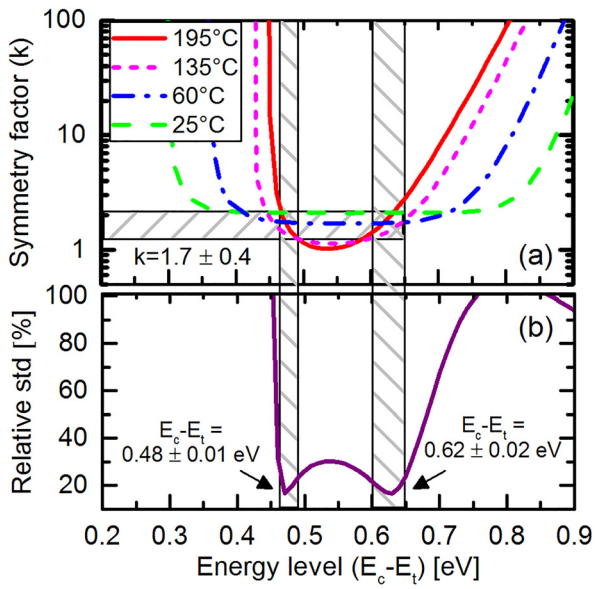

FIG. 5. DPSS analysis of the injection-dependent lifetime curves measured at varying temperatures. (a) Superposition of all DPSS-k curves in the same plot area. (b) Relative standard deviation (purple solid line) of the DPSS-k curves as a function of the energy level. The convergence of the curves to the common intersection points has been assessed in terms of relative standard deviation, whose minima define the optimal values of the energy level ($E_c - E_t = 0.48 \pm 0.01$ eV and $E_c - E_t = 0.62 \pm 0.02$ eV) and symmetry factor $k = 1.7 \pm 0.4$. The error margins have been estimated from the width of the minima of the curve representing relative standard deviation, i.e., a 10% tolerance range has been defined for each plateau and the uncertainty ranges for k and the energy level have been accordingly determined.

RIGHTSLINK

points. This is probably a consequence of the fit errors, the moderate capture asymmetry of the defect which confines the possible solutions to a narrow range of values and the slight variation of k across the temperature range imposed by the temperature-dependence of capture cross sections.

C. Temperature dependence of $\sigma_{n,p}$ and verification of LS results

In order to analyze the temperature dependence of capture cross sections and ascertain the validity of the previous spectroscopic results, the SRH model has been applied to the TDLS lifetime data. Figure 6(a) displays the temperature-dependent lifetime measured at the excess carrier density $\Delta n = 2 \times 10^{14}\,\mathrm{cm}^{-3}$, which corresponds to the lowest injection level at which the lifetime was reliably measured by the instrument across the temperature range. Since the shallow energy level has a negligible effect on the low-injection lifetime, the TDLS curve is fully described by a single SRH energy level. If capture cross sections are assumed to be temperature-independent, the best fit is achieved with a defect located in the upper half of the bandgap with an energy level of $E_c - 0.13\,\mathrm{eV}$ (Figure 6(b)).

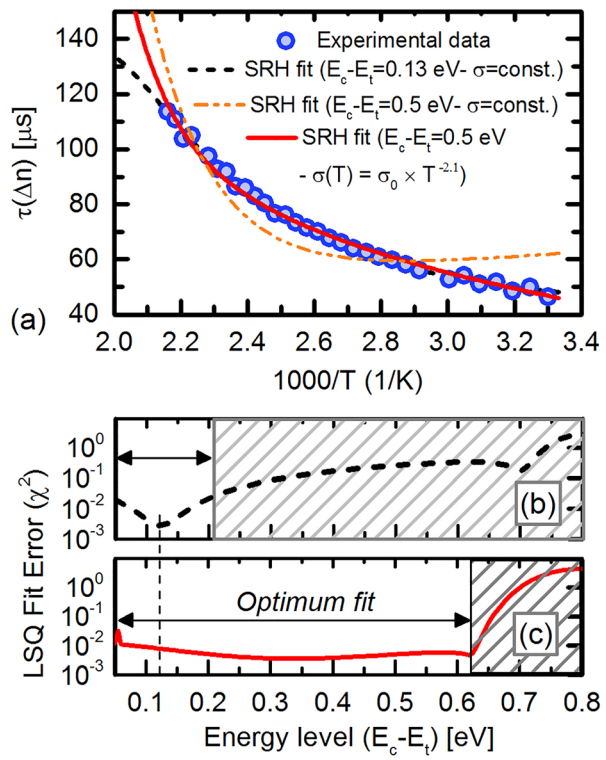

FIG. 6. Lifetime temperature dependence measured at a fixed injection level ($\Delta n = 2 \times 10^{14}\,\mathrm{cm}^{-3}$) in an intentionally Cu-contaminated p-type 3.4 Ω·cm FZ sample. (a) The experimental data (circles) are fitted to the SRH model assuming (i) a defect energy level $E_c - E_t = 0.13\,\mathrm{eV}$ with temperature independent capture cross sections (black dashed line), (ii) a deep recombination center at $E_c - E_t = 0.5\,\mathrm{eV}$ with temperature independent capture cross sections (orange dashed-dotted line), and (iii) energy level at $E_c - E_t = 0.5\,\mathrm{eV}$ with a power law temperature dependence $\sigma(T) = \sigma_0 \times T^{-2.1}$ (red solid line). ((b) and (c)) DPSS diagrams of the least squares fit error obtained with (solid red line) and without (dashed black line) the assumption of temperature-dependent capture cross sections. In the case of temperature-dependent capture cross sections, the optimum fit to the experimental data is obtained when the energy level $E_c - E_t < 0.61\,\mathrm{eV}$.

However, the IDLS result in Figure 4 indicates that the energy level must lie deeper in the band gap to allow a simultaneous fit to the injection- and temperature-dependent lifetime data, such that the spectroscopic information gained under the assumption of temperature-independent capture cross sections has to be rejected for reasons of inconsistency. As can be seen from Figure 6(a), if the defect energy level is assumed to be located near the mid-bandgap, the supposition of temperature independent capture cross sections leads to the overestimation of the LLI lifetime at room temperature. This suggests that the SRH model must be complemented with an appropriate parametrization that accounts for the enlargement of $\sigma_{n,p}$ at decreasing temperatures.[25] The optimum fit to the experimental data is obtained under the assumption of a power-law temperature dependence of the capture cross sections,[25] i.e., $\sigma(T) = \sigma_0 \times T^{-\alpha}$ with $\alpha = 2.1$. The identified $\sigma(T)-$ dependence will be further discussed in Sec. V.

Concerning the defect energy levels, the DPSS diagram in Figure 6(c) shows that the fitting error is minimized within the energy range between the conduction band edge and $E_c - 0.61\,\mathrm{eV}$, thus excluding most of the lower half of the bandgap from the possible energy levels associated with the deep recombination center. The domain of possible defect parameters that provide a consistent fit to both injection- and temperature-dependent curves is further restricted if the spectroscopic result from the IDLS curve in Figure 4 and the result of the TDLS analysis (Figure 6(c)) are superposed in the same graph, as indicated in Figure 7. The DPSS-k diagrams in Figure 7(a) show two specific intersection points located at E_c–0.49 eV and E_c–0.61 eV with a common symmetry factor $k = 2$, resulting in good agreement with the spectroscopic result that was previously discussed in Sec. IV B.

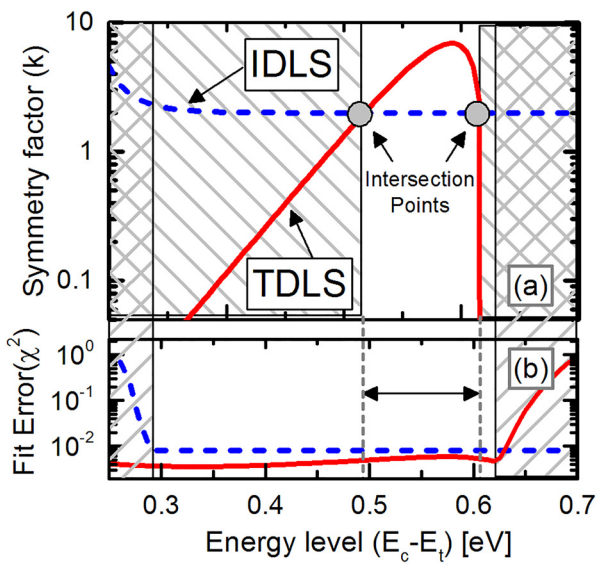

FIG. 7. Superposition of the DPSS diagrams extracted from the TDLS (solid red lines) and IDLS (dashed blue lines) lifetime data shown in Figures 4 and 6(c). (a) The intersection points of the DPSS-k curves (grey circles) indicate the defect parameters that provide an optimum fit to both IDLS and TDLS curves. (b) The fit error of both IDLS and TDLS is minimized within the energy range between E_c–0.28 eV and E_c–0.63 eV, thus confining the defect energy level within this energy interval.

RIGHTSLINK

D. LS results obtained with different specimens

In order to cross-check the spectroscopic results obtained thus far, LS analyses have been applied to a set of FZ wafers with varying doping concentrations. For all samples, the SRH fit required the assumption of two independent recombination centers, one of them being a shallow energy state located between $E_c - 0.1$ eV and $E_c - 0.2$ eV with $k = 0.1$.

Concerning the deep recombination center, Table I summarizes the SRH parameters fitted from the lifetime data of all samples, and the SRH fit of the lifetime data obtained at room temperature is shown in Fig. 8. It is possible to notice that the spectroscopic analysis led to the identification of similar values for both k and $E_c - E_t$, thus confirming the existence of energy states near the mid-bandgap with a moderate capture asymmetry. Furthermore, the SRH fit of all TDLS curves confirms the aforementioned $\sigma(T)$−dependence, which was modeled in terms of $\sigma(T) = \sigma_0 \times T^{-\alpha}$ with the exponent α varying between 1.2 and 2.1.

V. COMPARISON WITH LITERATURE DATA AND DISCUSSION

The spectroscopic analysis of the injection- and temperature-dependent lifetime data indicated the coexistence of at least two energy levels, i.e., a deep energy state located near the mid-bandgap and a shallow level in the upper bandgap half. Copper is known to give rise to a variety of complexes in silicon, some of which have been correlated with previously reported DLTS spectra. Interstitial copper (Cu_i^+) atoms and copper-boron (CuB) pairs are unlikely to affect the minority carrier lifetime, as no recombination activity has been related to such complexes.[27,28] Moreover, the concentration of Cu_i^+ has been observed to decrease during illumination,[29] thus indicating the transformation of Cu_i^+ into a different recombination-active defect. The formation of substitutional copper defects (Cu_s) during light soaking has been intensively discussed in the literature. Early contributions attributed Cu-LID to the dissociation of a recombination inactive pure copper complex, which was long presumed to be Cu_sCu_i pair, and the subsequent formation of highly recombination active Cu_s complexes.[14,30] However, this reaction does not explain the aforementioned decrease of Cu_i^+ concentration during light-soaking. Moreover, DLTS studies on intentionally Cu contaminated material revealed the existence of two acceptor energy states located at $E_v + 0.41\ldots0.45$ eV[31–34] and $E_c - 0.16$ eV[24] and a donor energy level at $E_v + 0.22$ eV,[24,35] which were later associated with the substitutional copper defect.[35] While the energy state at $E_c - 0.16$ eV seems to be in good agreement with LS results reported in this study, no strong evidence of the other energy states can be found. The acceptor-like behavior of the deep energy state at $E_v + 0.41\ldots0.45$ eV would impose a large capture cross section for majority carriers, and hence $k \ll 1$, which is in disagreement with the spectroscopic result that was shown in Sections IV B and IV C. Furthermore, the energy level of this recombination center seems not to match the result of the TDLS fit and the temperature-dependent DPSS analysis (Figures 5 and 6(c)), which set the energy level at least 100 meV deeper into the bandgap.

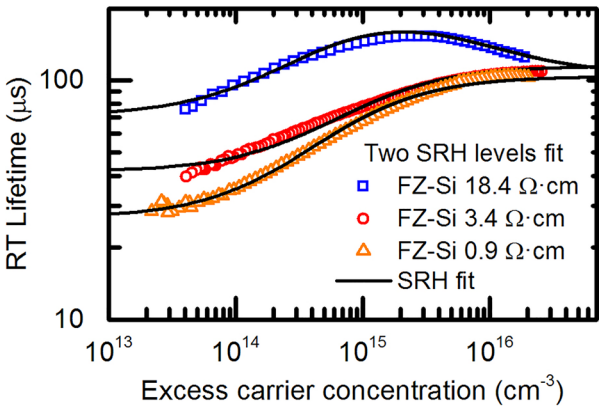

FIG. 8. Injection dependent lifetime curves measured at room temperature in Cu-contaminated samples featuring different doping concentrations. The solid line represents the fit obtained with two non-interacting SRH levels (deep and shallow).

Copper is also known to form electrically active copper silicides ($\eta'' - Cu_3Si$)[36] stemming from the precipitation of Cu_i^+ atoms. Such extended defects introduce a continuous band of energy states in the upper half of the bandgap, from $E_c - 0.15$ eV to $E_c - (0.4\ldots0.5)$ eV[37,38] with an estimated electron capture cross-section $\sigma_n = 3 \times 10^{-16}$ cm^2.[39] Macdonald *et al.* showed through LS methods that the impact of this distributed energy band can be approximated via two non-interacting SRH defects with energy levels located at $E_c - 0.15$ eV and $E_c - 0.58$ eV, which approximately correspond to the extremes of the aforementioned energy band.[40,41] Though some uncertainty on the actual energy levels exists, the spectroscopic result obtained in this work appears to be in good agreement with the IDLS and TDLS analysis presented by Macdonald *et al.* for thermally induced Cu precipitates. Considering that Cu precipitates introduce a continuous band of energy states rather than individual states due to their extended nature, it must be pointed out that a rigorous study of carrier recombination through distributed energy states would require more complex recombination models. This may explain the slight displacement

TABLE I. Overview of the defect parameters associated with the deep recombination center In Cu-contaminated FZ-Si samples with varying resistivity. The optimal defect parameters have been obtained by superposing the DPSS diagrams associated with all the temperature-dependent lifetime curves, as illustrated in Figure 5. The $\sigma(T)$-dependence was determined by fitting the SRH model to the TDLS lifetime data, as described in Sec. IV C.

Resistivity [Ω·cm]	p_0 [cm^{-3}]	DPSS solution 1 E_c−E_t [eV]	DPSS solution 2 E_c−E_t [eV]	$k^{DPSS-1,2}$	$\sigma(T)$
0.9	1.65×10^{16}	0.51 ± 0.02	0.61 ± 0.02	2.6 ± 0.4	$\propto T^{-1.2}$
3.4	4×10^{15}	0.48 ± 0.01	0.62 ± 0.02	1.7 ± 0.4	$\propto T^{-2.1}$
18.4	7.13×10^{14}	0.51 ± 0.03	0.59 ± 0.03	1.9 ± 0.3	$\propto T^{-1.9}$

RIGHTSLINK

between the experimental data and the fitted SRH lifetime, which is visible in Figures 3 and 8. Nevertheless, the results shown in this contribution indicate that the description of the lifetime data via the assumption of single point-like SRH energy states still provides a satisfactory approximation of the underlying recombination activity over the measurable injection range.

Based on the above defect identification, it is possible to relate the recombination mechanisms at metal precipitates to the aforementioned $\sigma(T)$-dependence and speculate on the effect of the degradation conditions (e.g., light intensity or temperature during LID) on the recombination activity of such defects. The $\sigma(T)$-dependence described in Sec. IV C is likely to arise from the temperature dependence of the thermionic recombination currents at the Schottky junction formed near the precipitate-semiconductor interface.[42] The aforementioned $\sigma(T)$-dependence has also been associated with the excitonic Auger capture process, which has been reported for defects introducing deep energy states.[43]

In addition to the doping concentration, the degradation kinetics of Cu-LID have been found to significantly dependent on other parameters, such as illumination intensity, temperature, and the presence of bulk defects (e.g., vacancies or dislocations).[7,15] All these parameters are likely to affect the precipitate size distribution and, therefore, result in a different recombination activity of such defects. In addition to providing further evidence of the existence of such precipitates, advanced recombination models that correlate the injection-dependent lifetime with the precipitate radius[44] may also provide additional information on the formation mechanisms.

VI. CONCLUSION

In this work, injection- and temperature-dependent lifetime spectroscopy analysis has been applied to intentionally Cu-contaminated *p*-type FZ silicon for characterizing the recombination activity of the defects activated under room-temperature illumination. In order to verify the accuracy and repeatability of the spectroscopic result, the analysis has been applied to a set of similarly processed wafers of different resistivities. For all samples, IDLS and TDLS methods revealed that the recombination activity of light-activated copper defects is well described by two non-interacting energy levels, i.e., a shallow energy level at $E_c - E_t = 0.1 - 0.2\,\text{eV}$ and a deep recombination center at $E_c - E_t = 0.48 - 0.51\,\text{eV}$ or $E_c - E_t = 0.59 - 0.62\,\text{eV}$ with k varying between 1.7 and 2.6 and a strong power-law temperature dependence of the capture cross sections. The defect energy levels coincide with the edges of the energy band associated with Cu-precipitates, thus indicating this defect as the possible culprit behind the observed LID process. Since lifetime spectroscopy methods are mostly sensitive to the defects that impact the recombination lifetime to a greater extent, the result shown in this work does not rule out the coexistence of other less-recombination active defects, which might be pinpointed by DLTS measurements.

ACKNOWLEDGMENTS

This research was performed at the Micronova Nanofabrication Centre of Aalto University. The authors acknowledge the support from the European Research Council under the European Union's FP7 Programme ERC Grant Agreement No. 307315. A.I. acknowledges the support of the Aalto ELEC doctoral school. J.L. acknowledges the Characterization and Modeling of Materials (CMM) Group at Karlstad University and Walter Ahlström Foundation.

[1]J. Schmidt and K. Bothe, "Structure and transformation of the metastable boron- and oxygen-related defect center in crystalline silicon," Phys. Rev. B **69**(2), 024107 (2004).
[2]V. V. Voronkov and R. Falster, "Light-induced boron-oxygen recombination centres in silicon: Understanding their formation and elimination," Solid State Phenom. **205–206**, 3–14 (2013).
[3]F. Fertig, K. Krauß, and S. Rein, "Light-induced degradation of PECVD aluminium oxide passivated silicon solar cells," Phys. Status Solidi -Rapid Res. Lett. **9**(1), 41–46 (2015).
[4]K. Ramspeck, S. Zimmermann, H. Nagel, A. Metz, Y. Gassenbauer, B. Brikmann, and A. Seidl, "Light induced degradation of rear passivated mc- Si solar cells," in Proceedings of the 27th EUPVSEC, 2012, pp. 861–865.
[5]H. Savin, M. Yli-Koski, and A. Haarahiltunen, "Role of copper in light induced minority-carrier lifetime degradation of silicon," Appl. Phys. Lett. **95**(15), 152111 (2009).
[6]J. Lindroos, Y. Boulfrad, M. Yli-Koski, and H. Savin, "Preventing light-induced degradation in multicrystalline silicon," J. Appl. Phys. **115**(15), 154902 (2014).
[7]A. Inglese, A. Focareta, F. Schindler, J. Schön, J. Lindroos, M. C. Schubert, and H. Savin, "Light-induced degradation in multicrystalline silicon: The role of copper," Energy Proc. **92C**, 808–814 (2016).
[8]J. Lindroos and H. Savin, "Formation kinetics of copper-related light-induced degradation in crystalline silicon," J. Appl. Phys. **116**(23), 234901 (2014).
[9]Y. Boulfrad, J. Lindroos, M. Wagner, F. Wolny, M. Yli-Koski, and H. Savin, "Experimental evidence on removing copper and light-induced degradation from silicon by negative charge," Appl. Phys. Lett. **105**(18), 182108 (2014).
[10]Y. Boulfrad, J. Lindroos, A. Inglese, M. Yli-Koski, and H. Savin, "Reduction of light-induced degradation of boron-doped solar-grade Czochralski silicon by Corona charging," Energy Proc. **38**, 531–535 (2013).
[11]H. Väinölä, M. Yli-Koski, A. Haarahiltunen, and J. Sinkkonen, "Sensitive copper detection in P-type CZ silicon using μPCD," J. Electrochem. Soc. **150**(12), G790 (2003).
[12]M. Yli-Koski, H. Väinölä, A. Haarahiltunen, J. Storgårds, E. Saarnilehto, and J. Sinkkonen, "Light activated copper defects in P-type silicon studied by PCD," Phys. Scr. **114**, 69–72 (2004).
[13]D. A. Ramappa, "Surface photovoltage analysis of phase transformation of copper in p-type silicon," Appl. Phys. Lett. **76**(25), 3756 (2000).
[14]W. B. Henley, D. A. Ramappa, and L. Jastrezbski, "Detection of copper contamination in silicon by surface photovoltage diffusion length measurements," Appl. Phys. Lett. **74**(2), 278 (1999).
[15]A. Inglese, J. Lindroos, and H. Savin, "Accelerated light-induced degradation for detecting copper contamination in p-type silicon," Appl. Phys. Lett. **107**(5), 052101 (2015).
[16]S. Rein, T. Rehrl, W. Warta, and S. W. Glunz, "Lifetime spectroscopy for defect characterization: Systematic analysis of the possibilities and restrictions," J. Appl. Phys. **91**(4), 2059 (2002).
[17]D. Macdonald and A. Cuevas, "Validity of simplified Shockley-Read-Hall statistics for modeling carrier lifetimes in crystalline silicon," Phys. Rev. B **67**, 075203 (2003).
[18]W. Shockley and W. T. Read, "Statistics of the recombinations of holes and electrons," Phys. Rev. **87**(5), 835–842 (1952).
[19]R. N. Hall, "Electron-hole recombination in germanium," Phys. Rev. **87**(2), 387 (1952).
[20]J. M. Dorkel and P. Leturcq, "Carrier mobilities in silicon semi-empirically related to temperature, doping and injection level," Solid State Electron. **24**(9), 821–825 (1981).
[21]J. S. Blakemore, *Semiconductor Statistics* (Oxford, 1962).
[22]D. Macdonald and A. Cuevas, "Trapping of minority carriers in multicrystalline silicon," Appl. Phys. Lett. **74**(12), 1710 (1999).
[23]M. A. Green, "Intrinsic concentration, effective densities of states, and effective mass in silicon," J. Appl. Phys. **67**(6), 2944 (1990).

RIGHTSLINK

[24]J. Lindroos and H. Savin, "Review of light-induced degradation in crystalline silicon solar cells," Sol. Energy Mater. Sol. Cells **147**, 115–126 (2016).
[25]S. Rein, *Lifetime Spectroscopy* (Springer-Verlag, Berlin/Heidelberg, 2005), Vol. 85.
[26]S. Rein and S. W. Glunz, "Electronic properties of interstitial iron and iron-boron pairs determined by means of advanced lifetime spectroscopy," J. Appl. Phys. **98**(11), 113711 (2005).
[27]A. A. Istratov and E. R. Weber, "Physics of copper in silicon," J. Electrochem. Soc. **149**(1), G21 (2002).
[28]A. A. Istratov, C. Flink, H. Hieslmair, T. Heiser, and E. R. Weber, "Influence of interstitial copper on diffusion length and lifetime of minority carriers in p-type silicon," Appl. Phys. Lett. **71**(15), 2121 (1997).
[29]A. Belayachi, T. Heiser, J. P. Schunck, and A. Kempf, "Influence of light on interstitial copper in p-type silicon," Appl. Phys. A **80**(2), 201–204 (2005).
[30]I. Tarasov and O. Ostapenko, "Light induced defect reactions in boron-doped silicon: Cu versus Fe," in Proceedings of the 8th Workshop on Crystalline Silicon Solar Cell Material and Process (1998), p. 207.
[31]M. Saritas and A. Peaker, "Deep states associated with oxidation induced stacking faults in RTA p-type silicon before and after copper diffusion," Solid State Electron. **38**(5), 1025–1034 (1995).
[32]S. D. Brotherton, J. R. Ayres, A. Gill, H. W. van Kesteren, and F. J. A. M. Greidanus, "Deep levels of copper in silicon," J. Appl. Phys. **62**(5), 1826 (1987).
[33]H. Lemke, "Substitutional transition metal defects in silicon grown-in by the float zone technique," in Proceedings of the Fourth International Symposium on High Purity Silicon (1996), p. 272.
[34]A. Mesli and T. Heiser, "Defect reactions in copper-diffused and quenched *p* -type silicon," Phys. Rev. B **45**(20), 11632–11641 (1992).
[35]K. Graff, *Metal Impurities in Silicon-Device Fabrication* (Springer, Berlin, Heidelberg, 2000), Vol. 24.
[36]W. Schröter, V. Kveder, M. Seibt, H. Ewe, H. Hedemann, F. Riedel, and A. Sattler, "Atomic structure and electronic states of nickel and copper silicides in silicon," Mater. Sci. Eng. B **72**(2–3), 80–86 (2000).
[37]M. Seibt, M. Griess, A. A. Istratov, H. Hedemann, A. Sattler, and W. Schröter, "Formation and properties of copper silicide precipitates in silicon," Phys. Status Solidi **166**(1), 171–182 (1998).
[38]A. A. Istratov, H. Hedemann, M. Seibt, O. F. Vyvenko, W. Schröter, T. Heiser, C. Flink, H. Hieslmair, and E. R. Weber, "Electrical and recombination properties of copper-silicide precipitates in silicon," J. Electrochem. Soc. **145**(11), 3889 (1998).
[39]M. Seibt, R. Khalil, V. Kveder, and W. Schröter, "Electronic states at dislocations and metal silicide precipitates in crystalline silicon and their role in solar cell materials," Appl. Phys. A **96**(1), 235–253 (2009).
[40]D. Macdonald, A. Cuevas, S. Rein, P. Lichtner, and S. W. Glunz, "Temperature- and injection-dependent lifetime spectroscopy of copper-related defects in silicon," in *Proceedings of 3rd World Conference on Photovoltaic Energy Conversion* (IEEE, 2003), Vol. 1.
[41]D. Macdonald, W. Brendle, A. Cuevas, and A. A. Istratov, "Injection-Dependent Lifetime Studies of Copper Precipitates in Silicon," in Proceedings of the Workshop on Crystalline Silicon Solar Cell Materials and Processes (2002), pp. 201–204.
[42]M. D. Negoita and T. Y. Tan, "Metallic precipitate contribution to generation and recombination currents in p-n junction devices due to the Schottky effect," J. Appl. Phys. **94**(8), 5064 (2003).
[43]A. Hangleiter, "Nonradiative recombination via deep impurity levels in semiconductors: The excitonic Auger mechanism," Phys. Rev. B **37**(5), 2594–2604 (1988).
[44]W. Kwapil, J. Schon, W. Warta, and M. C. Schubert, "Carrier recombination at metallic precipitates in p-and n-type silicon," IEEE J. Photovoltaics **5**(5), 1285–1292 (2015).

RIGHTSLINK